

On the large role of weak uncorrelated pinning introduced by BZO nanorods at low temperatures in REBCO thin films

A. Xu,^{1,*} V. Braccini,² J. Jaroszynski,¹ Y. Xin,¹ and D. C. Larbalestier¹

¹*National High Magnetic Field Laboratory, Florida State University, Tallahassee, Florida 32310*

²*CNR-SPIN, Corso Perrone 24, I-16152 Genova, Italy*

(Dated: June 21, 2018)

REBa₂Cu₃O_x films can achieve remarkably high critical current density values by the incorporation of insulating nanoparticles. A particular interesting case concerns BaZrO₃ (BZO) nanorods, whose strongly correlated effect is seen at high temperatures. Here we investigate the field, temperature and angular dependence of the critical current density over a wide temperature range from 4.2 K to 77 K, and magnetic fields up to 31 T. We show that the correlated *c*-axis pinning of BZO nanorods becomes progressively less obvious at lower temperature. Indeed at 4.2 K and fields up to 31 T, the only correlated pinning is for fields parallel to the film plane. We interpret the change as being due to significant contributions from dense but weak pins that thermal fluctuations render ineffective at high temperatures but which become strong at lower temperatures.

PACS numbers: 74.25.Wx, 74.25.Sv 74.78.-w, 74.72.-h

I. INTRODUCTION

REBa₂Cu₃O_x (REBCO, where RE = rare earth) thin films are very promising high temperature superconductors for applications because of their high current-carrying capability in very strong magnetic fields over a wide operating temperature regime. Higher and less anisotropic critical currents I_c still remain very desirable for widespread applications.¹ Fortunately, it has been demonstrated that several approaches work for the I_c improvement, including increasing the thickness of the REBCO layer,^{2,3} mitigating the weak-link effect of grain boundaries⁴⁻⁶ and by better understanding and more effective enhancement of the pinning mechanisms.⁷

Enhancement of flux pinning by optimization of nanoscale defects is fundamental to J_c improvement.^{1,7-9} More specifically, it was first established that oxygen deficiencies were the governing pinning centers in high quality YBCO single crystals.^{10,11} In turn, dislocations and point defects were found to be strong pins at low temperatures and important for the typically observed one or two order of magnitude higher J_c of YBCO thin films.^{12,13} Compared to the growth defects mentioned above, intentionally introduced pinning centers have captured more attention due to their high tunability. In early study of the pinning effects of heavy-ion irradiation on YBCO single crystals large J_c increases at all temperature and magnetic fields, especially for magnetic field parallel to the irradiation direction was found.¹⁴ Later, self-assembled BaZrO₃ nanorods lying along the *c*-axis were incorporated into YBCO thin films and coated conductors. BZO has a high lattice mismatch, a high melting temperature, and it is insoluble in REBCO, all of which contribute to the substantial improvement of J_c over a wide angular range far from the *c*-axis.¹⁵ A series of Ba-metal oxide (BMO, where M = Sn, Hf and Ir) second phases acting as correlated *c*-axis pinning effects were explored thereafter in order to decrease the anisotropic

J_c .¹⁶⁻¹⁸ Unfortunately, the additions of BMO are detrimental to T_c and thus degrade the properties at liquid nitrogen temperature. However, Harrington *et al.*¹⁹ obtained excellent pinning properties while keeping T_c at 92 K even with very high concentrations of self-assembled RE₃TaO₇ (RE = Er, Gd and Yb) nanorods, where, unlike the tensile stress-inducing BZO, the RE₃TaO₇ introduces a compressive stress on the REBCO.¹⁹ More recently, an 0.5 μ m thick pulsed laser deposition (PLD) YBCO film with embedded double perovskite Ba₂YNbO₆ nanorods showed a maximum flux pinning force density $F_{p,max}$ in excess of 30 and 120 GN/m³ at 75.5 K and 65 K.²⁰ Such $F_{p,max}$ values exceed a long challenged benchmark, that of 18-20 GN/m³ found in the best pinning-tailored NbTi wire at $T = 4.2$ K.²¹

In general the maximum J_c of any superconductor is limited by the depairing current density $J_d = \phi_0 / 3\sqrt{3}\pi\mu_0\lambda^2\xi$ according to anisotropic Ginzburg-Landau theory.^{7,22} Here ϕ_0 is the flux quantum, λ is the London penetration length, ξ is the coherence length and μ_0 is the vacuum permeability. In fact REBCO films can clearly exert strong pinning, as shown by estimates that $\sim 30\%$ of J_d is achieved in YBCO thin films, at least at low fields.²³ But high field magnets do require further J_c improvement by flux pinning engineering of REBCO conductors. In spite of REBCO having by far the highest irreversibility fields $H_{irr}(T)$ of all cuprate superconductors, neither $H_{irr}(T)$ nor $J_c(H)$ are high enough for making magnets of 5–10 T unless the temperature is reduced below ~ 30 –40 K. So far, most pinning studies have been concentrated on J_c enhancement at high temperatures, 65 K to 77 K, and magnetic fields near self-field for power transmission. However, potential applications of REBCO conductors extend over much broader temperature and magnetic field regimes.^{1,24} Recently, thanks to the availability of REBCO conductor with suitable mechanical properties, the development of all-superconducting magnets above 25 T at 4.2 K became feasible, and some prototypes greater than 30 T were demonstrated.²⁴⁻²⁶

However, coil design depends on understanding the detailed angular dependence of J_c over broad temperature and field ranges so that safe coil quench design can be predicted with confidence. Moreover, superconducting magnetic storage systems, motors and generators, working at intermediate temperatures ~ 30 K, are important potential applications too.^{27–29} Thus, a systematic study of the pinning mechanisms over a broad range covering all applications regimes is indispensable for both practical and fundamental reasons.

BZO nanorods are well known to produce strong correlated c -axis pinning at high temperatures. Surprisingly, however, recent studies of samples containing BZO nanorods showed no signs of c -axis correlated pinning at 4.2 K, even though $J_c(H)$ was strongly enhanced.^{30,31} Here we show that the dominant 4.2 K pinning characteristic, valid up to at least 31 T, can be fit to a standard anisotropic mass scaling except near the ab -plane where correlated pinning, probably by the CuO charge-reservoir layers enhances J_c . By measuring the angular-dependent current density $J_c(\theta)$ over a wide range of field and temperature, we observe that this uncorrelated pinning is valid only below ~ 30 K. We conclude that these low temperature angular-independent pins are largely point pins induced by the strain fields of the BZO nanorods. Because they are point pins, they are easily thermally depinned at higher temperatures, leaving the strong correlated c -axis pinning effects of the BaZrO₃ nanorods then quite evident. At 4.2 K, however, the point pins contribute almost half of the J_c .

II. EXPERIMENTAL DETAILS

We performed an extensive angular $J_c(\theta, T, H)$ characterization of a recent REBCO thin film in fields up to 31 T and temperatures from 4.2 to 77 K. The 1.1 μm thick film was grown by metal-organic chemical vapor deposition (MOCVD) on a high strength metal alloy tape commercially available as Hastelloy, on which a buffer layer textured by ion-beam assisted deposition (IBAD) was deposited. A ~ 2 μm thick sputtered silver layer was deposited on the REBCO layer as protection and intermediate electrical contact layer for the ~ 50 μm thick copper layer, which was electro-plated on it.³² This sample is representative of the most advanced coated conductor made by SuperPower Inc. The Zr addition produces BZO nanorods with an equivalent flux density $B_\phi \approx 3$ T. Earlier study has shown that such films have high J_c properties at both high and low temperatures.³¹

The 4.2 K and high field four-probe critical current measurements were performed in a 52 mm cold bore 15 T superconducting magnet and the 52 mm warm bore 31 T Bitter magnet, fitted with a 38 mm bore liquid He cryostat. The 10 K to 77 K measurements were carried out in a 16 T Physical Property Measurement System (PPMS). Samples were rotated with respect to the external magnetic field around the axis parallel to the current

direction to maintain a maximum Lorentz force configuration. The angle $\theta = 0$ is defined as the applied magnetic field perpendicular to the tape plane which is parallel to the crystallographic c -axis direction with a typical uncertainty of $1 - 4^\circ$ caused by an offset caused by the IBAD process.^{30–32}

Due to the high critical current (I_c) values observed at lower temperatures, samples with different geometries were prepared in order to avoid harmful Joule heating and overstressing by the large Lorentz forces ($I_c \times B$) possible in different regimes of temperature and magnetic field. A 50×500 μm bar was cut by Nd-YAG (yttrium aluminum garnet) laser for the J_c measurement at 77 K. Even narrower samples, ~ 10 μm wide and 200 μm long were patterned by SEM/FIB so as to restrict I_c to ≤ 5 A when the sample was measured in helium gas between 10 and 70 K. In both cases, copper and silver layers were removed by wet-etching. Larger bridges about ~ 1 mm wide and 1 cm long were patterned leaving the silver and copper layers present for the 4.2 K measurements. Two different home-made I_c probes equipped with rotating sample platforms were used. One had a maximum current-carrying capability of ~ 500 A for high I_c measurement in liquid helium, while the second had ~ 5 A capability in the PPMS cryostat for studies at temperatures above 10 K.

TEM images were taken in a JEOL JEM 2011 transmission electron microscope. The critical temperature (T_c) is defined as the temperature where resistance R equals zero. The 77 K irreversibility field was determined from the field dependence of J_c with the criterion $J_c = 100$ A/cm². For lower temperatures where $H_{irr}(T)$ is greater than magnetic field available $H_{irr}(T)$ was assessed from the formula in³³.

III. RESULTS

The MOCVD sample under study has critical temperature $T_c = 90.7$ K. The nominal composition of this sample is Y_{0.6}Gd_{0.6}Ba₂Cu_{2.3}O_x with 7.5 at. % Zr doping, composition found to give the highest in-field J_c values at 77 K.³² The sample has J_c as high as 3.4 MA/cm² at self-field and 1.0 MA/cm² at 1 T, at $\theta = 0^\circ$. Even more importantly, both the irreversibility field, $H_{irr} = 10.2$ T, and the maximum flux pinning force, $F_{p\max} = 12$ GN/m³ along the c -axis are substantially higher than that of other REBCO films with similar thickness, ~ 1 μm .

Figure 1 shows a typical cross-sectional, bright-field TEM image of this MOCVD sample. BZO nanorods, with ~ 8 nm diameter, with inclinations of $\sim 5 - 20^\circ$ to the c -axis are quite obvious. Their density corresponds to a matching field $B_\phi = \phi_0/a^2 \sim 2.6$ T, where $a \approx 28$ nm is the measured average distance between the BZO nanorods and $\phi_0 = h/2e \approx 2.1 \times 10^{-15}$ Wb is the flux quantum. Such nanorods are responsible for the broad I_c maxima observed at elevated temperatures when H is off the film plane. This strong correlated pinning pro-

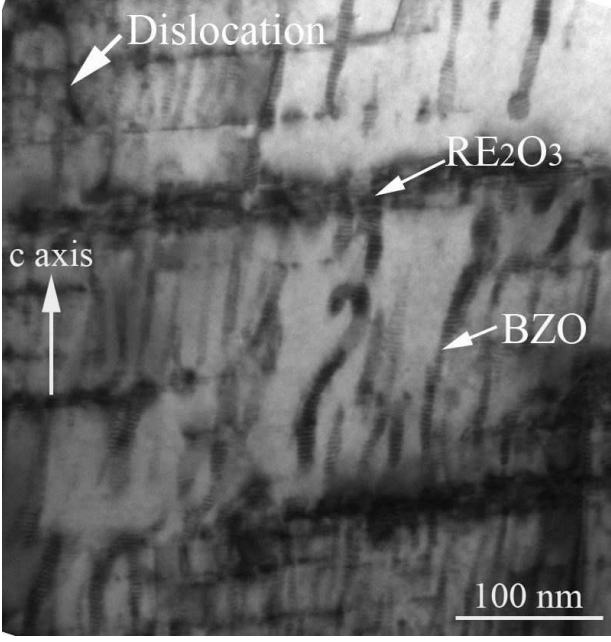


FIG. 1: Cross-sectional TEM image of the MOCVD sample. Splayed BZO nanorods along c -axis and tilted RE_2O_3 precipitate arrays along ab -plane are the major visible correlated pinning centers. The RE_2O_3 precipitates are effective 3D pins that enhance J_c at all orientations. A low density of threading dislocations that are effective pins along the c -axis are also visible in this image.

duces the outstanding superconducting performance observed at 77 K. Moreover, a high density of self-assembled RE_2O_3 precipitate arrays aligned along the ab -plane is another important source of pinning.^{33–35} Interestingly, TEM observation indicates that the ab -plane of REBCO tilts $\sim 2^\circ$ from the buffer layer because of the IBAD process while the RE_2O_3 precipitate arrays tilt away from the ab -plane by $\sim 5^\circ$, as previously reported.³³ Threading dislocations provide additional c -axis correlated pinning, although we believe that, their contribution is negligible compared to BZO nanorods because of their low density.

Figure 2 (a) presents the c -axis field dependence $J_c(H||c)$ for magnetic fields up to 16 T or 31 T at various temperatures from 4.2 K to 77 K. For $T = 77$ K, only data below the irreversibility field, $H_{irr} = 10.2$ T are plotted. $J_c(H)$ shows less field dependence with decreasing temperature. At 10 K, J_c at self-field reaches 43 MA/cm² which corresponds to $\sim 17\%$ of J_d . J_c at 16 T and 10 K is as high as 3.7 MA/cm² equal to the self-field J_c at 77 K. At 4.2 K, J_c decreases from 33.3 MA/cm² at 1 T to 2.9 MA/cm² at 31 T. These high current densities correspond to $I_c = 1.5$ kA at 1 T and 0.13 kA at 31 T for standard production 4 mm wide tape. Such high I_c values make effective characterization of such conductors difficult. Notably, this MOCVD BZO-containing sample shows higher J_c at all temperatures below ~ 70 K than optimized NbTi wire evaluated at 4.2 K.²¹ The power-

law dependence of J_c on magnetic field, $J_c \propto H^{-\alpha}$, is observed at low temperatures. At 4.2 K, the power-law exponent $\alpha = 0.7$ describes J_c well in the whole 1 – 31 T range of magnetic field.

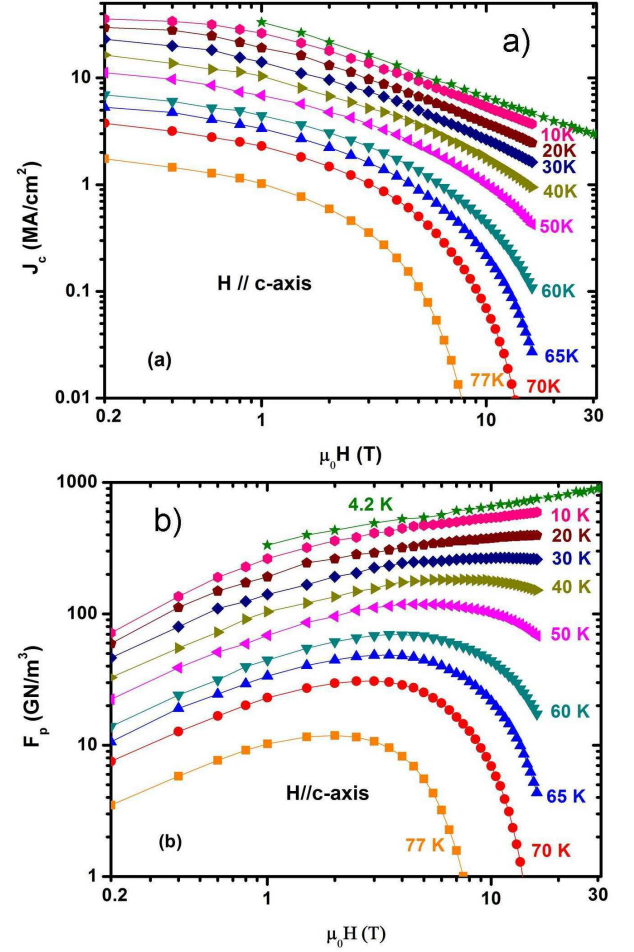


FIG. 2: (color online) (a) Field dependence of J_c for H parallel to the c -axis at temperatures between 4.2 K and 77 K and magnetic fields up to 31 T and (b) The corresponding flux pinning force calculated from $F_p = J_c \times \mu_0 H$. Only data below H_{irr} is shown at $T = 77$ K in (a). $J_c \propto H^{-\alpha}$ is observed at temperatures below ~ 30 K. It can be seen that $F_{p,max}$ is trending to more than 1 TN/m³ at the lowest temperature. Lines connecting data points are guides for the eyes.

Figure 2 (b) shows flux pinning force density $F_p = J_c \times \mu_0 H$ as a function of external magnetic field parallel to the c -axis at various temperatures. The superior F_p values confirm the strong pinning provided by the defects existing in this sample. The highest measured F_p at 4.2 K and 31 T almost reaches 1000 GN/m³. This is the record high value observed in any superconductor so far. It is also striking that the pinning force above 4 T at 30 K barely depends on magnetic field. The maximum pinning force is ~ 267 GN/m³ at 30 K while at lower temperatures F_p maxima correspond to fields higher than 16 T (or even 31 T at 4.2 K) and could not be observed experimentally.

The double-peaked $F_p(H)$ dependence shown by BZO-doped YBCO PLD thin films on SrTiO_3 single crystal substrates³⁶ are not observed in the present work at any temperature.

The angular dependence of J_c is a powerful tool for understanding pinning mechanisms and also crucial for magnet design. Figure 3 presents $J_c(\theta, 1 \text{ and } 4 \text{ T})$ of the MOCVD sample at 77 K, 50 K, 30 K and 10 K. J_c maxima around the c -axis are clearly seen at 77 K and 50 K. These maxima do not occur exactly at 0° due to the splayed inclination of the BZO nanorods. At 1 T and 77 K, the c -axis J_c reaches 1.1 MA/cm^2 , about one third higher than the J_c maximum value around the ab -plane and twice the minimum J_c close to the ab -plane. As the magnetic field increases to 4 T, the c -axis J_c peak becomes lower than the ab -peak, because the field exceeds the matching field of 2.6 T, corresponding to the BZO nanorod density. It is worth noting that both BZO nanorods and the RE_2O_3 precipitate arrays contribute to J_c at 77 K, being responsible for the c -axis peak and for J_c enhancement over the whole angular range especially around the ab -plane. Comparing the 77 K to lower temperature data at the same field, the c -axis peak becomes less distinct as temperature decreases, not being observable at all at temperatures below 30 K. This strongly suggests that the dominant pinning mechanism changes at lower temperatures and that the crossover temperature is $\sim 30 \text{ K}$. The ratio of $J_c||c$ and $J_c||ab$ decreases from 1.4 at 77 K to 0.9 at 50 K, showing the reversion to that expected by the mass anisotropy at low temperature. At lower temperature, the $J_c||ab$ peak becomes more evident, indicating a strengthening of the ab -plane correlated pinning. At low fields $J_c||ab$ varies from a cusplike dependence above 50 K to a smooth, Ginzburg-Landau (GL)-like peak at lower temperatures and at 10 K from GL-like at low fields to cusp-like at high magnetic fields.

Ultra high-field magnet applications at 4.2 K are an important area for applications of YBCO conductors, for which we have performed studies of $J_c(\theta)$ up to 31 T.^{30,31} Figure 4 shows the angular dependence of J_c of this MOCVD sample at 4.2 K up to 25 T. Evidently, the c -axis J_c peak is totally washed out at 4 K at all fields from 3 T up to 25 T. As noted also in the contest of data taken at 10 K, the GL-like $J_c(\theta)$ dependence evolves towards a cusp-like for magnetic fields above $\sim 5 \text{ T}$.

IV. DISCUSSION

The temperature and magnetic field dependence of the flux pinning force for many superconductors often obeys a scaling relation, as was first proposed by Fietz and Webb^{21,37}:

$$F_p(T, H) = \text{const} \times [H_{c2}(T)]^n g(h) \quad (1)$$

in which the exponent n describes the temperature dependence of the upper critical field $H_{c2}(T)$ or in this case

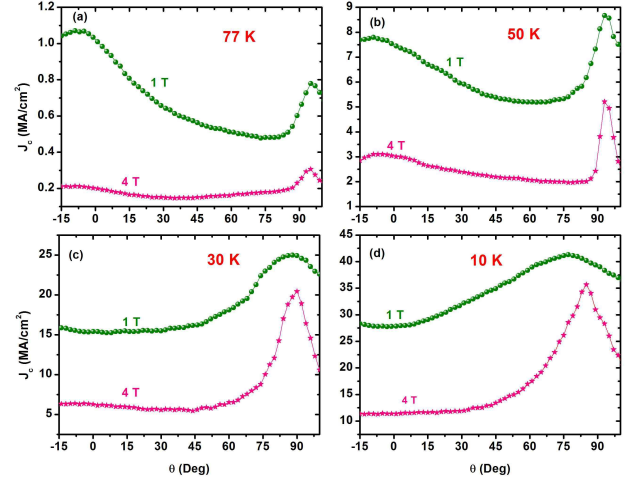


FIG. 3: (color online) $J_c(\theta)$ at (a) 77 K, (b) 50 K, (c) 30 K and (d) 10 K and magnetic fields up to 4 T for H parallel to the c -axis. The c -axis J_c peak caused by the BZO nanorods is evident at 77 K and 1 T but becomes progressively less obvious with increasing magnetic field or decreasing temperature. Below 30 K, the peak is completely unobservable at any magnetic field.

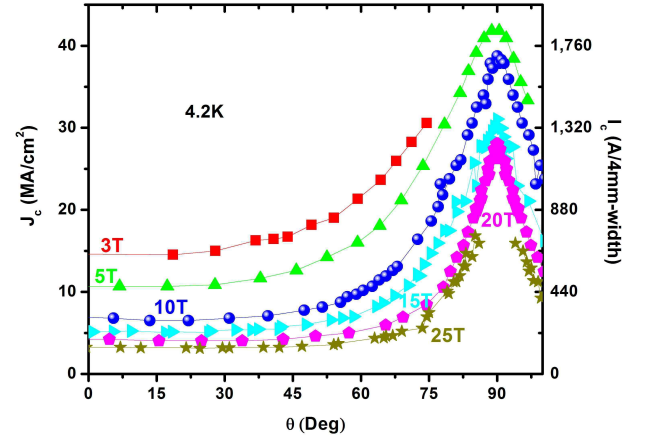


FIG. 4: (color online) $J_c(\theta)$ at 4.2 K under magnetic fields up to 25 T. The c -axis J_c peak is totally washed out, while the J_c peak around the ab -plane becomes narrower with increasing magnetic field. More importantly, this MOCVD BZO-containing sample shows higher J_c and a broader J_c around the ab -peak than MOCVD samples without BZO nanorods.

the irreversibility field $H_{irr}(T)$ and $g(h)$ is a pinning function which, in simple cases where the dominant pinning mechanisms are temperature-independent, depends only on the reduced field h ($h = H/H_{irr}(T)$). We first address the extent to which this simple pinning assumption is valid for this strong pinning sample over such a broad range of T and H

The reduced pinning force density, F_p/F_{pmax} as a function of reduced field h is plotted in Fig. 5 (a) using a reduced field defined as $h = H/H_{irr}(T)$, instead of $h = H/H_{c2}(T)$ for low temperature superconductors.²¹

In both cases the result is the same: the scaling field is defined for the field at which J_c tends to zero. At $T = 77$ K, $F_p/F_{p\max}$ peaks at $h = 0.2$ and $H = 2.0$ T, which is close to the matching field of 2.6 T for BZO nanorods in this sample. On decreasing temperature from 77 K to 50 K, the peak h_{\max} shifts to lower reduced field, from 0.2 to 0.15, indicating that there is no simple correlation between h_{\max} and B_ϕ . With further temperature decrease to 30 K, there is no obvious change of the peak position. However, the reduced peak width broadens as the temperature is lowered to 40 K and then to 30 K. Thus, exact temperature scaling does not occur in this sample, as is further demonstrated in Fig. 5 (b) by plotting $\log F_p$ vs. $\log H_{irr}(T)$ at varying reduced fields. The scaling exponent n increases from 1.65 to 2.06 as the reduced field rises from 0.25 to 0.75. However, excellent temperature scaling is observed at constant reduced field, as shown by the linear dependence of $\log F_p$ on $\log H_{irr}(T)$. Taken together, both figures indicate that the dominant pinning mechanism(s) are varying with temperature.

More compelling evidence for the temperature dependence of the pinning mechanisms is provided by the temperature dependence of J_c/J_d , the ratio of the measured pinning critical current density to the calculated depairing current density, which may be used as a convenient measure of the effectiveness of the pinning defects in the phenomenology of type II superconductors.⁷ In this work, we use J_c/J_d to track the pinning strength variation with temperature. Figure 6 presents J_c/J_d for H parallel to the c -axis as a function of temperature at several different magnetic fields, where J_d is obtained from the following equation^{38,39}

$$J_d(T, H) = J_d(0, 0) \left(1 - \frac{T}{T_c}\right)^{3/2} \left(1 - \frac{H}{H_{c2}(T)}\right)^{3/2} \quad (2)$$

Here $J_d(0, 0) = 300$ MA/cm² (Ref. 38) and $H_{c2}(T) = H_{c2}(0)[1 - (T/T_c)^2]$. $T_c = 91$ K and $H_{c2}(0, H||c) = 121$ T.⁴⁰ In the more often used self-field limit, this expression reduces to the usual equation $J_d = \phi_0/3\sqrt{3}\pi\mu_0\lambda^2\xi$.

Two evident features are observed in Fig. 6. First, it is clear that the ratio J_c/J_d continuously declines with increasing temperature for all fields evaluated from 1–16 T, signaling that thermal fluctuations are important even in this strong pinning regime.^{11,22,41,42} However, the dominant regime for thermal fluctuations appears to vary with magnetic field. At the lowest field evaluated, 1 T, it appears that three temperature regimes can be observed. On raising the temperature from 4.2 K, there is an initially steep drop of J_c/J_d up to about 30 K, the rate of decrease then flattening between about 30 and 65 K, before finally falling off more rapidly again at the highest temperatures. The transition to strong thermal fluctuations regime seems to occur at ~ 65 K at 1 T, 60 K at 4 T, 50 K at 8 T and 40 K at 16 T. The steep, low temperature fall in J_c/J_d appears at all fields, which suggests

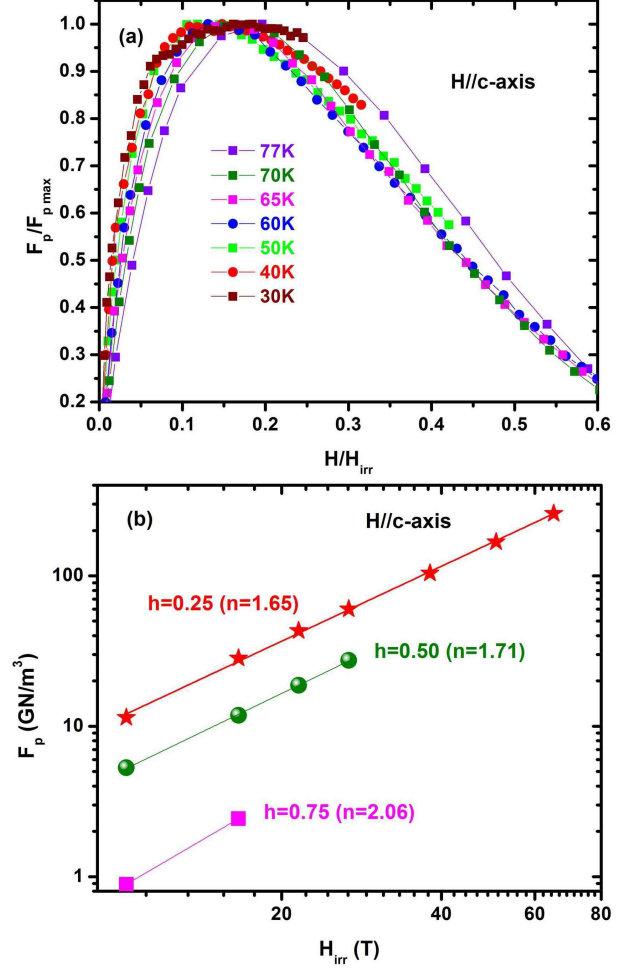


FIG. 5: (color online) (a) Reduced pinning force, $F_p/F_{p\max}$ for H parallel to the c -axis as a function of reduced field H/H_{irr} at temperature from 30 K to 77 K showing the lack of a perfect temperature scaling of F_p . (b) The scaling of F_p as a function of irreversibility field at several reduced magnet fields shows good temperature scaling at constant reduced field, although the scaling exponent is not independent of reduced field.

that an additional pinning mechanism operating only at low temperatures is present. However, the contribution of this pinning mechanism is strongly suppressed by both increasing temperature and increasing field, so that at 16 T its effect is only weakly visible as a point of inflection at 10 – 15 K on the $J_c/J_d(T)$ plot.

More details of the low temperature pinning and high temperature pinning can be obtained by plotting $\log J_c$ vs. T and $\log J_c$ vs. T^2 . Flux pinning can be categorized as strong or weak based on the extent of the distortion of the flux line lattice by the pinning defects. It has been shown that the J_c determined by weak pinning mechanisms decays as an exponential function of temperature while J_c of strong pinning decays as an exponential function of T^2 .^{42–46} Accordingly, Fig. 7 (a) plots $\log J_c$ vs. T^2 . J_c indeed decays as an exponential function of T^2

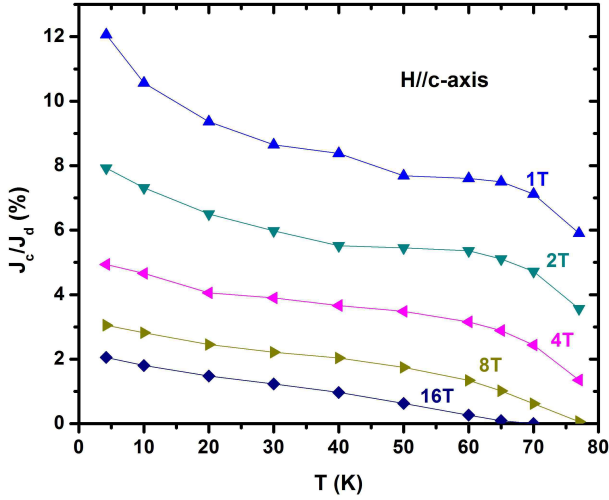


FIG. 6: (color online) The ratio of transport and depairing current densities J_c/J_d for H parallel to the c -axis as a function of temperature at fields of 1-16 T. Three temperature regimes of $J_c(H, T)$ are visible. Starting from low temperature, $J_c(H, T)$ falls steeply before moderating between about 30 to 60 K (at 1 T), then falling off again very steeply at $\sim 60 - 80$ K.

in the intermediate temperature regime of 30 – 65 K at 1 T, 30 – 60 K at 4 T, 30 – 50 K at 8 T and 12 T, but it is also clear that there is an “excess” J_c at the lowest temperatures which quickly disappears at high temperature. Consistent with plot of J_c/J_d vs. T in Fig. 6, we also observe a sharp drop of J_c at high temperature. At lower temperatures, as shown in Fig. 7 (b), the exponential decay of J_c , shown by the linear dependence of $\log J_c$ on T , is observed below ~ 40 K at 1 T and 4 T and below ~ 30 K at 8 T and 12 T. This analysis clearly suggests that additional weak pinning is present below ~ 30 K. In the $\sim 30 - 60$ K range, stronger pinning centers then control J_c until even these strong pins are rendered ineffective by increasing thermal fluctuations at higher temperatures. The strong pinning provided by the BZO nanorods and RE_2O_3 precipitates in this sample significantly raise the crossover temperature at which thermal fluctuations dominate from ~ 60 K, as compared to ~ 30 K in YBCO single crystal samples.⁴¹ The BZO nanorods and RE_2O_3 precipitates provide strong pinning at $\sim 30 - 60$ K as clearly shown by multiple other studies.^{45,47,48}

Further information about the additional low temperature weak pinning can be obtained by analysis of the angular dependence of J_c at 4.2 K using the anisotropic scaling approach⁷ proposed by Civalé et al.⁴⁹ If the pinning is due to uncorrelated defects randomly distributed over angular space, then J_c should depend on H and θ only through a single variable $J_c(H, \theta) = J_c[H\varepsilon(\theta)]$ where $\varepsilon(\theta) = [\cos^2(\theta) + \gamma^{-2}\sin^2(\theta)]^{1/2}$, where γ^2 is the electronic mass anisotropy parameter. Since we have observed that J_c follows $J_c \propto H^{-\alpha}$ at low temperature especially at 4.2 K, as shown in Fig. 2 (a), then $J_c(H, \theta) \propto [H\varepsilon(\theta)]^{-\alpha}$.

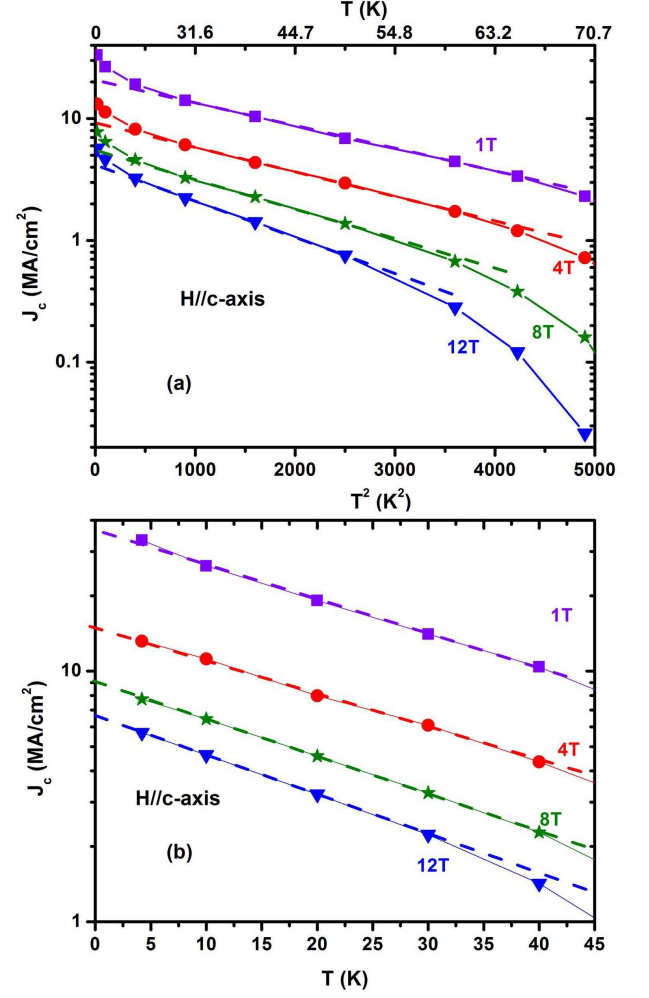


FIG. 7: (color online) Plot of (a) $\log J_c$ vs. T^2 and (b) $\log J_c$ vs. T for H parallel to the c -axis. A linear dependence of $\log J_c$ on T^2 characteristic of strong pinning is observed in the intermediate temperature range $\sim 30 - 60$ K in (a) while the linear dependence of $\log J_c$ on T characteristic of weak pinning is observed at low temperature below ~ 30 K in (b). Taken together the plots indicate that weak pinning is adding to the strong pinning provided by RE_2O_3 and BZO up to about 30 K and that the strong pins then dominate J_c until strong thermal fluctuations take over above about 65 K (at 1 T).

Power law behavior with $\alpha \approx 0.7$ for BZO-containing samples and $\alpha \approx 0.5$ for non-BZO samples was reported by us previously.³¹ Figure 8 presents $J_c(\theta)$ at 5, 15 and 25 T using the anisotropic scaling parameters $\alpha = 0.7$ and $\gamma = 3$. These curves give a reasonable fit of the data in the low angle region, from 0° up to about $60 - 70^\circ$, leading us to conclude that, over this wide range all around the c -axis where the correlated effects of the BZO nanoparticles are so evident at higher temperatures, the pinning is indeed uncorrelated and random. Clearly the most reasonable interpretation of this behavior is that the *additional* pinning that operates only up to 30 – 40 K

dominates over the strong pinning effect of the BZO nanorods at lower temperatures. It is interesting that the scaling suggests an effective anisotropy $\gamma = 3$ that is less than the H_{c2} anisotropy $= 5$ expected from the intrinsic mass anisotropy $\gamma^2 = 25 - 30$. The reasons for this behavior are unclear at this time, but smaller anisotropy is positive in any case of applications. It is interesting that $\gamma = 3$ is also an excellent fit to the very broad study of the angular variation of $H_{irr}(T)$ for a very similar sample over the range about 55-80 K and H up to 45 T.⁵⁰ In this case the effective γ was evaluated in the limit that the pin strength goes to zero, rather than in the very finite pin strength limit assessed here, implying a rather consistent behavior over a wide range of the superconducting phase space.

The power law dependence of J_c on H has been reported in many works^{48,51}. However, the increase of α from 0.5 (no nanorods) to 0.7 at 4.2 K when BZO nanorods are present is in contrast to high temperature observations where the presence of BZO nanorods decreases α .^{31,48} This is yet more evidence that different pinning mechanisms operate at high and low temperatures.

Based on the above analysis, we propose that BZO additions lead to a significant density of strain-induced, weak pins that cannot resist thermal fluctuation much above about 30 K. Since they do operate at all fields up to 31 T at 4.2 K, it is clear that they are much denser than the strong BZO and RE_2O_3 pins. Due to the strong effects of increasing field and temperature, we assume that these highly effective pins are dense but point pins (effective size of the order of ξ^3 or less, where ξ is the coherence length). Our earlier 4.2 K comparison of non-BZO and BZO-containing samples up to 31 T showed two significant features: One was that the BZO samples have significantly higher J_c while the second was that the enhancement disappeared by 30 – 35 T, certainly a high field but actually only about 25 % of H_{irr} or H_{c2} at 4.2 K. Here our variable temperature examination of the BZO sample shows that the uncorrelated pinning effects produced by the point pins are only visible up to ~ 30 K. Both characterizations show that the pin strength decays rapidly with increasing H and T , consistent with them being small and easily thermally depinned. As Fig. 1 shows, only the larger BZO and RE_2O_3 strong pins are visible in TEM, so we do not yet have a measure of the point pin concentration. But we can reasonably infer that their density must be high, since they are able to completely hide the effect of the BZO nanorods, even at fields below B_ϕ (compare the $J_c(1 \text{ T})$ data at 77 and 10 K in Figs. 3a and 3d). Indeed, the depressed T_c of MOCVD and PLD YBCO samples induced by BZO nanorods has recently been attributed to oxygen deficiencies introduced by strain imposed by the lattice mismatch between BZO nanorods and the YBCO matrix.⁵²

The specific supporting evidence was provided by atomic-resolution Z-contrast imaging and electron energy loss spectroscopy which showed oxygen deficiencies surrounding BZO nanorods, a finding which also supports our proposal for the presence of dense point pins. Thus the overall conclusion of our study is extremely positive: the splayed BZO nanorods found in this coated conductor provide strong correlated pinning to enhance J_c around c -axis, a result shown in numerous studies in the 50-77 K range, but they also greatly add to the lower temperature J_c by additionally inducing dense but weak isotropic pinning by strain-induced point defects that raise J_c in the whole angular range at fields up to at least 31 T at 4.2 K where thermal depinning effects are small.

V. CONCLUSIONS

In this paper, we presented a very detailed $J_c(H, T, \theta)$ characterization of a modern, very high critical current density REBCO thin film containing $\sim c$ -axis oriented BZO nanorods and ab -plane RE_2O_3 pinning arrays over an exceptionally broad temperature (4.2 – 77 K) and magnetic field range (0 – 31 T). Analyzing the J_c data we studied the pinning evolution on temperature associated with BZO nanorods. An important new conclusion is that weak isotropic pinning from point defects produced by the strain field around BZO nanorods dominates J_c at low temperatures. More specifically, we observed that the usual c -axis J_c peak caused by BZO nanorods disappears with decreasing temperature, and vanishes completely below ~ 30 K. At 4.2 K, we found that J_c along the c -axis decays as $J_c \propto H^{-\alpha}$ with magnetic field up to 31 T. Although J_c decays faster with magnetic field compared with samples without BZO nanorods at 4.2 K, it is still higher at field up to at least 31 T. At low temperatures, the c -axis J_c peak is not seen at any magnetic field and the only correlated pinning present occurs around the ab -plane.

Acknowledgments

We are very grateful to colleagues in the HTS R&D group at the NHMFL who have provided many valuable comments and discussions, especially Alex Gurevich, David Hilton, Fumitake Kametani, and Chiara Tarantini. Some aspects of this work were supported by the Department of Energy, Office of Electric Delivery and Energy Research (grant number: DE-FC07-08ID14916) and some by the National High Magnetic Field Laboratory, which is supported by NSF Cooperative Agreement DMR-0654118 and by the State of Florida.

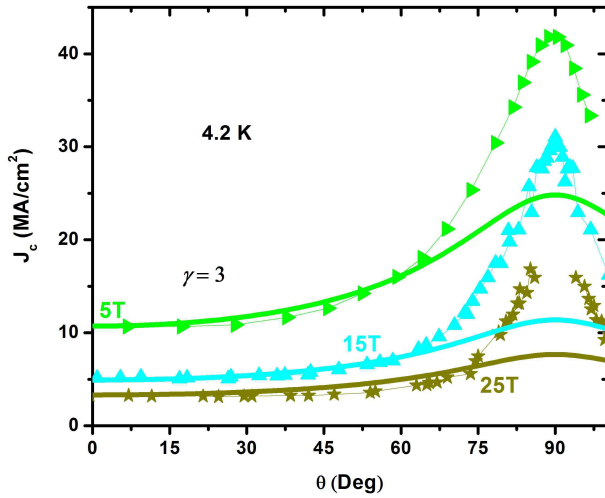


FIG. 8: (color online) Angular dependence of J_c (symbols) and J_c calculated from anisotropic G-L scaling model (thick lines) at 4.2 K and magnetic fields 5, 15 and 25 T. Anisotropic G-L scaling describes well the experimental data over a broad angular range up to, $\sim 0 - 60^\circ$ with $\alpha = 0.7$ and $\gamma = 3$. Thus, the weak uncorrelated pinning contributes to J_c at 4.2 K except in the vicinity of the ab -plane where intrinsic pinning is important.

-
- * Electronic address: aixiaxu@magnet.fsu.edu
- ¹ D. C. Larbalestier, A. Gurevich, D. M. Feldmann, and A. Polyanskii, *Nature* **414**, 368 (2001).
 - ² J. L. MacManus-Driscoll, A. Kursumovic, J. H. Durrell, S. Harrington, S. C. Wimbush, B. Maiorov, L. Stan, H. Zhou, T. Holesinger, and H. Wang, *IEEE Appl. Supercond.* **19**, 3180 (2009).
 - ³ V. Glyantsev, J. Huh, J. Dawley, P. Turner, C. Yung, B. Moeckly, B. Maiorov, Y. Coulter, C. Sheehan, and V. Matias (2011), proceedings of the MRS Spring 2011 Meeting, to be published.
 - ⁴ G. A. Daniels, A. Gurevich, and D. C. Larbalestier, *Appl. Phys. Lett.* **77**, 3251 (2000).
 - ⁵ G. Hammerl, A. Schmehl, R. R. Schulz, B. Goetz, H. Bielefeldt, C. Schneider, H. Hilgenkamp, and J. Mannhart, *Nature* **407**, 162 (2000).
 - ⁶ D. M. Feldmann, T. G. Holesinger, R. Feenstra, C. Cantoni, W. Zhang, M. Rupich, X. Li, J. H. Durrell, A. Gurevich, and D. C. Larbalestier, *J. Appl. Phys.* **102**, 083912 (2007).
 - ⁷ G. Blatter, M. V. Feigel'man, V. B. Geshkenbein, A. I. Larkin, and V. M. Vinokur, *Rev. Mod. Phys.* **66**, 1125 (1994).
 - ⁸ S. R. Foltyn, L. Civale, J. L. M.-D. Q. X. Jia, B. Maiorov, H. Wang, and M. Maley, *Nat. Mater.* **6**, 631 (2007).
 - ⁹ T. G. Holesinger, L. Civale, B. Maiorov, D. M. Feldmann, J. Coulter, D. J. Miller, V. A. Maroni, Z. Chen, D. C. Larbalestier, R. Feenstra, et al., *Adv. Mater.* **20**, 391 (2008).
 - ¹⁰ M. Daeumling, J. M. Seuntjens, and D. C. Larbalestier, *Nature* **346**, 332 (1990).
 - ¹¹ J. Vargas and D. C. Larbalestier, *Appl. Phys. Lett.* **60**, 1741 (1992).
 - ¹² B. Dam, J. M. Huijbregtse, F. C. Klaassen, R. C. F. van der Geest, G. Doornbos, J. H. Rector, A. M. Testa, S. Freisem, J. C. Martinez, B. Stäuble-Pmpin, et al., *Nature* **399**, 439 (1999).
 - ¹³ T. L. Hylton and M. R. Beasley, *Phys. Rev. B* **41**, 11669 (1990).
 - ¹⁴ L. Civale, A. D. Marwick, T. K. Worthington, M. A. Kirk, J. R. Thompson, L. Krusin-Elbaum, Y. Sun, J. R. Clem, and F. Holtzberg, *Phys. Rev. Lett.* **67**, 648 (1991).
 - ¹⁵ J. L. MacManus-Driscoll, S. R. Foltyn, Q. X. Jia, H. Wang, A. Serquis, L. Civale, B. Maiorov, M. E. Hawley, M. P. Maley, and D. E. Peterson, *Nat. Mater.* **3**, 439 (2004).
 - ¹⁶ S. Yasunaga, M. Mukaida, A. Ichinose, S. Horii, R. Teranishi, K. Yamada, K. Matsumoto, R. Kita, Y. Yoshida, and N. Mori, *Physica C* **468**, 1858 (2008).
 - ¹⁷ J. Hänisch, C. Cai, R. Hühne, L. Schultz, and B. Holzapfel, *Appl. Phys. Lett.* **86**, 122508 (2005).
 - ¹⁸ S. Engel, T. Thersleff, R. Hühne, L. Schultz, B. Holzapfel, S. Engel, T. Thersleff, L. Schultz, B. Holzapfel, and L. Schultz, *Appl. Phys. Lett.* **90**, 102505 (2007).
 - ¹⁹ S. A. Harrington, J. H. Durrell, B. Maiorov, H. Wang, S. C. Wimbush, A. Kursumovic, J. H. Lee, and J. L. MacManus-Driscoll, *Supercond. Sci. Technol.* **22**, 022001 (2009).
 - ²⁰ D. M. Feldmann, T. G. Holesinger, B. Maiorov, S. R. Foltyn, J. Y. Coulter, and I. Apodaca, *Supercond. Sci. Technol.* **23**, 095004 (2010).
 - ²¹ C. Meingast and D. C. Larbalestier, *J. Appl. Phys.* **66**, 5971 (1989).
 - ²² A. Gurevich, *Supercond. Sci. Technol.* **20**, S128 (2007).
 - ²³ M. Miura, B. Maiorov, S. A. Baily, N. Haberkorn, J. O. Willis, K. Marken, T. Izumi, Y. Shiohara, and L. Civale, *Phys. Rev. B* **83**, 184519 (2011).

- ²⁴ H. Weijers, U. Trociewitz, W. Markiewicz, J. Jiang, D. Myers, E. Hellstrom, A. Xu, J. Jaroszynski, P. Noyes, Y. Viouchkov, et al., *IEEE Appl. Supercond.* **20**, 576 (2010).
- ²⁵ W. D. Markiewicz, H. W. Weijers, P. D. Noyes, U. P. Trociewitz, K. W. Pickard, W. R. Sheppard, J. J. Jaroszynski, A. Xu, D. C. Larbalestier, and D. W. Hazelton, *AIP Conference Proceedings* **1218**, 225 (2010).
- ²⁶ U. Trociewitz et al. (2011), submitted.
- ²⁷ Q. Li (2011), proceedings of the MRS Spring 2011 Meeting, to be published.
- ²⁸ K. Nagao, T. Nakamura, T. Nishimura, Y. Ogama, N. Kashima, S. Nagaya, K. Suzuki, T. Izumi, and Y. Shiohara, *Supercond. Sci. Technol.* **21**, 015022 (2008).
- ²⁹ M. Iwakuma, Y. Hase, T. Satou, A. Tomioka, M. Konno, Y. Iijima, T. Saitoh, Y. Yamada, T. Izumi, and Y. Shiohara, *IEEE Appl. Supercond.* **18**, 689 (2008).
- ³⁰ A. Xu, J. Jaroszynski, F. Kametani, Z. Chen, D. C. Larbalestier, Y. L. Viouchkov, Y. Chen, Y. Xie, and V. Selvamanickam, *Supercond. Sci. Technol.* **23**, 014003 (2010).
- ³¹ V. Braccini, A. Xu, J. Jaroszynski, Y. Xin, D. C. Larbalestier, Y. Chen, G. Carota, J. Dackow, I. Kesgin, Y. Yao, et al., *Supercond. Sci. Technol.* **24**, 035001 (2011).
- ³² V. Selvamanickam, Y. Chen, I. Kesgin, A. Guevara, T. Shi, Y. Yao, Y. Qiao, Y. Zhang, Y. Zhang, G. Majkic, et al., *IEEE Appl. Supercond.* **21**, 3049 (2011).
- ³³ Z. Chen, F. Kametani, Y. Chen, Y. Xie, V. Selvamanickam, and D. C. Larbalestier, *Supercond. Sci. Technol.* **22**, 055013 (2009).
- ³⁴ Z. J. Chen, D. M. Feldmann, D. C. Larbalestier, T. G. Holesinger, X. Li, W. Zhang, and M. W. Rupich, *Appl. Phys. Lett.* **91**, 052508 (2007).
- ³⁵ X. Song, Z. Chen, S. Kim, D. M. Feldmann, D. Larbalestier, J. Reeves, Y. Xie, and V. Selvamanickam, *Appl. Phys. Lett.* **88**, 212508 (2006).
- ³⁶ A. Augieri, G. Celentano, V. Galluzzi, A. Mancini, A. Rufoloni, A. Vannozzi, A. A. Armenio, T. Petrisor, L. Ciontea, S. Rubanov, et al., *J. Appl. Phys.* **108**, 063906 (2010).
- ³⁷ W. A. Fietz and W. W. Webb, *Phys. Rev.* **178**, 657 (1969).
- ³⁸ R. G. Boyd, *Phys. Rev.* **145**, 255 (1966).
- ³⁹ W. Lang, I. Puica, K. Siraj, M. Peruzzi, J. Pedarnig, and D. Buerle, *Physica C* **460-462**, 827 (2007).
- ⁴⁰ T. Sekitani, N. Miura, S. Ikeda, Y. Matsuda, and Y. Shiohara, *Physica B* **346-347**, 319 (2004).
- ⁴¹ M. V. Feigel'man and V. M. Vinokur, *Phys. Rev. B* **41**, 8986 (1990).
- ⁴² S. Senoussi, M. Osséna, G. Collin, and I. A. Campbell, *Phys. Rev. B* **37**, 9792 (1988).
- ⁴³ D. K. Christen and R. Thompson, *Nature* **364**, 98 (1993).
- ⁴⁴ J. Plain, T. Puig, F. Sandiumenge, X. Obradors, and J. R. Rabier, *Phys. Rev. B* **65**, 104526 (2002).
- ⁴⁵ T. Puig, J. Gutierrez, A. Pomar, A. Llorde, J. Gzquez, S. Ricart, F. Sandiumenge, and X. Obradors, *Supercond. Sci. Technol.* **21**, 034008 (2008).
- ⁴⁶ Ö. Polat, J. W. Sinclair, Y. L. Zuev, J. R. Thompson, D. K. Christen, S. W. Cook, D. Kumar, Y. Chen, and V. Selvamanickam, *Phys. Rev. B* **84**, 024519 (2011).
- ⁴⁷ J. Gutiérrez, A. Llorde, J. Gzquez, M. Gibert, N. Rom, S. Ricart, A. Pomar, F. Sandiumenge, N. Mestres, T. Puig, et al., *Nat. Mater.* **6**, 367 (2007).
- ⁴⁸ B. Mayorov, S. A. Baily, H. Zhou, O. Ugurlu, J. A. Kennison, P. C. Dowden, T. G. Holesinger, S. R. Foltyn, and L. Civale, *Nat. Mater.* **8**, 398 (2009).
- ⁴⁹ L. Civale, B. Mayorov, A. Serquis, J. O. Willis, J. Y. Coulter, H. Wang, Q. X. Jia, P. N. Arendt, M. Jaime, J. L. MacManus-Driscoll, et al., *J. Low Temp. Phys.* **135**, 87 (2004).
- ⁵⁰ C. Tarantini, J. Jaroszynski, F. Kametani, Y. L. Zuev, A. Gurevich, Y. Chen, V. Selvamanickam, D. C. Larbalestier, and D. K. Christen (2011), submitted.
- ⁵¹ Y. L. Zuev, D. K. Christen, S. H. Wee, A. Goyal, and S. W. Cook, *Appl. Phys. Lett.* **93**, 172512 (2008).
- ⁵² C. Cantoni, Y. Gao, S. H. Wee, E. D. Specht, J. Gazquez, J. Meng, S. J. Pennycook, and A. Goyal, *ACS Nano* **5**, 4783 (2011).